THE ROYAL SOCIETY

On the existence of flexural edge waves on submerged elastic plates

BY I. DAVID ABRAHAMS[1] AND ANDREW N. NORRIS[2]

[1]*Department of Mathematics, University of Manchester,*
Oxford Road, Manchester M13 9PL, UK
[2]*Department of Mechanical and Aerospace Engineering, Rutgers University,*
98 Brett Road, Piscataway, NJ 08854-8058, USA

The existence of flexural waves confined to the free edge of a fluid-loaded plate is established theoretically. Whereas analogous *in vacuo* edge waves exist for all parameter values, submerged plates are shown herein to support such waves only under very light fluid-loading conditions. For example, thin plates of aluminium, brass or Plexiglas will not support edge waves in water, although edge waves are permissible for each of these materials in air. The analysis is based on classical thin-plate theory and employs the Wiener–Hopf technique to derive the dispersion relation for the edge-wave wavenumber as a function of frequency. In the limit of zero fluid loading the dispersion relation predicts the well-known result of Konenkov for edge waves on thin plates *in vacuo*.

Keywords: structural acoustics; Wiener–Hopf technique; elastic plate; edge waves

1. Introduction

Thin elastic plates *in vacuo* with a free edge support flexural edge waves with wave speed proportional to and slightly less than the speed of flexural waves on a plate of infinite extent. This phenomenon was predicted independently by Konenkov (1960), Thurston & McKenna (1974) and Sinha (1974), all using the classical theory of thin-plate flexural motion. Subsequent experiments demonstrated the existence of the edge wave (Lagasse & Oliner 1976) with wave speed as predicted by theory, although the behaviour of the wave speed at higher frequencies is better modelled using a refined theory, such as the Mindlin plate theory (Norris *et al.* 2000). The edge wave is similar to a Rayleigh wave in that it decays exponentially with distance from the free edge, and wave energy is confined to the vicinity of the edge and propagates parallel to the edge. The speed of the edge wave is only marginally less than the flexural wave speed with a constant of proportionality that tends to unity as the Poisson's ratio vanishes. The edge wave is also predicted by more 'exact' analyses (finite-element method), and is also present in anisotropic thin plates (Norris 1994).

All of these studies, theoretical and experimental, ignored the influence of fluid loading. In practical situations, flexural plate motion almost always occurs in the presence of an exterior fluid (Cannell 1976), except in extraordinary circumstances, such as structures in outer space! The purpose of this paper is to examine whether

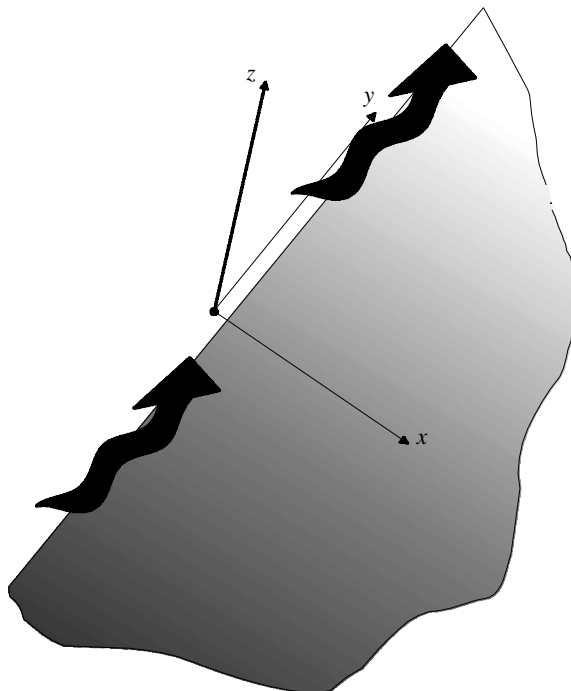*Proc. R. Soc. Lond.* A (2000) **456**, 1559–1582

1559

Figure 1. The dimensionless Cartesian coordinate system (2.12) showing the thin
elastic plate occupying $x > 0$, and the direction of propagation of the edge wave.

unattenuated edge waves can exist in the presence of a fluid, or whether the enveloping fluid radiates energy in a direction perpendicular to the edge. To answer this question most easily we restrict our study to the thin-plate theory for an isotropic material in an inviscid fluid. The problem is defined in § 2 and solved in § 3. The nature of the acoustic far-field is examined in § 4, while the existence of edge waves is discussed in § 5, and illustrated by numerical examples for practical material combinations. Concluding remarks are offered in § 6.

2. Formulation of the eigenvalue problem

(a) The physical problem

As mentioned above, the model under consideration is composed of a thin elastic plate of semi-infinite extent immersed in a compressible fluid (see figure 1). Defining Cartesian coordinates $(\hat{x}, \hat{y}, \hat{z})$, then the plate occupies the region $\hat{x} > 0$, $-\infty < \hat{y} < \infty$, $\hat{z} = 0$, and the deflections on it are governed (see, for example, Junger & Feit 1986) by

$$D\left(\frac{\partial^2}{\partial \hat{x}^2} + \frac{\partial^2}{\partial \hat{y}^2}\right)^2 \hat{w} + \rho_{\mathrm{p}} h \frac{\partial^2 \hat{w}}{\partial \hat{t}^2} = -\hat{p}|_{-}^{+}, \qquad (2.1)$$

where $\hat{w}(\hat{x}, \hat{y}, \hat{t})$ is the displacement in the $\hat{z}$-direction and $\hat{p}|_{-}^{+}$ is the pressure jump,

$$\lim_{\varepsilon \to 0}[\hat{p}(\hat{x}, \hat{y}, +\varepsilon, \hat{t}) - \hat{p}(\hat{x}, \hat{y}, -\varepsilon, \hat{t})],$$

across the plate. The latter loading is exerted by the fluid, which occupies the infinite region exterior to the plate. This fluid is taken as inviscid and compressible, and it undergoes small motions about its stationary ambient state and so can be described in terms of a velocity potential, $\hat{\phi}$, defined from the velocity field

$$\hat{\boldsymbol{u}} = \left(\frac{\partial}{\partial \hat{x}}, \frac{\partial}{\partial \hat{y}}, \frac{\partial}{\partial \hat{z}} \right) \hat{\phi}. \tag{2.2}$$

Hence, the pressure can be expressed as

$$\hat{p} = -\rho_{\mathrm{f}} \frac{\partial \hat{\phi}}{\partial \hat{t}}. \tag{2.3}$$

The potential itself satisfies

$$\frac{\partial^2 \hat{\phi}}{\partial \hat{x}^2} + \frac{\partial^2 \hat{\phi}}{\partial \hat{y}^2} + \frac{\partial^2 \hat{\phi}}{\partial \hat{z}^2} = \frac{1}{c^2} \frac{\partial^2 \hat{\phi}}{\partial \hat{t}^2}, \tag{2.4}$$

and the plate displacement is related to the velocity potential through

$$\frac{\partial \hat{w}}{\partial \hat{t}} = \frac{\partial \hat{\phi}}{\partial \hat{z}}. \tag{2.5}$$

In (2.1), the constants are ρ_{p}, the plate density, and D, the plate bending stiffness, which may be written in terms of Poisson's ratio, ν, and Young's modulus, E, for the solid material as well as the plate thickness h, namely:

$$D = \frac{Eh^3}{12(1 - \nu^2)}. \tag{2.6}$$

The fluid is characterized by its speed of sound c and its density ρ_{f}. The plate is free on the edge $x = 0$; that is, there are no applied forces or moments, and so (Graff 1975) the deflection must satisfy the edge constraints:

$$\frac{\partial^2 \hat{w}}{\partial \hat{x}^2} + \nu \frac{\partial^2 \hat{w}}{\partial \hat{y}^2} = 0, \quad \hat{x} = 0, \tag{2.7}$$

$$\frac{\partial^3 \hat{w}}{\partial \hat{x}^3} + (2 - \nu) \frac{\partial^3 \hat{w}}{\partial \hat{x} \partial \hat{y}^2} = 0, \quad \hat{x} = 0. \tag{2.8}$$

A travelling-wave solution is sought in which the wave propagates without attenuation in the $\hat{y}$-direction, and its energy is confined to the vicinity of the plate edge. That is, disturbances in the plate decay to zero as $\hat{x} \to \infty$,

$$\hat{w}(\hat{x}, \hat{y}, \hat{t}) \to 0, \quad \hat{x} \to \infty, \tag{2.9}$$

and also in the fluid

$$\hat{\phi} \to 0, \quad \hat{\nabla}\hat{\phi} \to 0, \quad |\hat{x}^2 + \hat{z}^2| \to \infty. \tag{2.10}$$

Therefore, the model is essentially an eigenvalue problem, where the positive real wavenumber for waves propagating in the $\hat{y}$-direction is sought for zero forcing.

(b) Non-dimensional parameters

Before solving the above system, it is useful to non-dimensionalize. If a bending wave propagates along the plate (2.1) with angular frequency ω, the *in vacuo* displacements have wavenumber

$$\mu = \left(\frac{\rho_\mathrm{p} h \omega^2}{D}\right)^{1/4}. \tag{2.11}$$

Thus, μ^{-1} is an appropriate length-scale and ω^{-1} is a suitable time-scale to scale the boundary-value problem upon

$$x = \hat{x}\mu, \qquad y = \hat{y}\mu, \qquad z = \hat{z}\mu, \qquad t = \hat{t}\omega, \tag{2.12}$$

and the dependent variables are scaled according to

$$w = \hat{w}\mu, \qquad \phi = \hat{\phi}\left(\frac{\mu^2}{\omega}\right), \qquad p = \hat{p}\left(\frac{\mu^2}{\omega^2 \rho_\mathrm{f}}\right). \tag{2.13}$$

We now seek travelling-wave solutions of the form

$$\phi(x, y, z, t) = \mathrm{Re}\{\psi(x, z)\exp[\mathrm{i}k\mu\hat{y} - \mathrm{i}\omega\hat{t}]\} = \mathrm{Re}\{\psi(x, z)\exp[\mathrm{i}ky - \mathrm{i}t]\}, \tag{2.14}$$
$$w(x, y, t) = \mathrm{Re}\{\eta(x)\exp[\mathrm{i}ky - \mathrm{i}t]\}, \tag{2.15}$$

where the reduced dependent variables $\psi(x, z)$, $\eta(x)$ can, respectively, by substitution, be shown to satisfy

$$\frac{\partial^2 \psi}{\partial x^2} + \frac{\partial^2 \psi}{\partial z^2} + (k_0^2 - k^2)\psi = 0, \tag{2.16}$$

for (x, z) exterior to the plate from (2.4), in which k_0 is the dimensionless fluid wavenumber

$$k_0 = \omega/\mu c, \tag{2.17}$$

and

$$\left\{\left(\frac{\mathrm{d}^2}{\mathrm{d}x^2} - k^2\right)^2 - 1\right\}\eta(x) = -\mathrm{i}\tau[\psi(x, 0+) - \psi(x, 0-)], \qquad x > 0, \tag{2.18}$$

from (2.1), where

$$\tau = \frac{\rho_\mathrm{f}\omega^2}{D\mu^5} = \frac{\rho_\mathrm{f}/\rho_\mathrm{p}}{h\mu} \tag{2.19}$$

is a dimensionless *fluid-loading* parameter. Note that this quantity τ depends on frequency and on the thickness of the plate. It will later be shown to be useful to define a *frequency-independent* non-dimensional *fluid-loading* parameter ϵ, where

$$\epsilon = \frac{\rho_\mathrm{f}}{c}\left(\frac{E}{12(1 - \nu^2)\rho_\mathrm{p}^3}\right)^{1/2}. \tag{2.20}$$

This parameter is also independent of the plate thickness. In terms of ϵ, it may be shown that

$$\tau = \epsilon/k_0, \tag{2.21}$$

and

$$k_0 = \sqrt{\omega/\omega_c}, \tag{2.22}$$

where the coincidence frequency $\omega_c = 2\pi f_c$, at which the acoustic wavenumber equals that for *in vacuo* bending waves on the plate ($k_0 = 1$) is given by

$$\omega_c = \frac{\rho_f c}{\rho_p h \epsilon}. \tag{2.23}$$

The free-edge constraints for the plate (2.7), (2.8) along $x = 0$ may now be expressed as

$$\frac{d^2\eta}{dx^2}(0) - k^2\nu\eta(0) = 0, \tag{2.24}$$

$$\frac{d^3\eta}{dx^3}(0) - k^2(2-\nu)\frac{d\eta}{dx}(0) = 0, \tag{2.25}$$

where the quantities specified here, i.e. $\eta(x)$ and its first three derivatives, must remain bounded at the tip $x = 0$. Plate deflection and fluid potential are related, via (2.5) and continuity of normal velocity across $z = 0$, by

$$\eta(x) = i\frac{\partial\psi}{\partial z}(x, 0+) = i\frac{\partial\psi}{\partial z}(x, 0-), \quad x > 0, \tag{2.26}$$

and it is noted that $\psi(x, z)$ is continuous across $z = 0$, $x < 0$, but has a jump determined by (2.18) on $x > 0$, i.e. across the plate. Therefore, symmetry in the governing equations implies that ψ is an odd function of z, so, for simplicity, attention may be restricted to $z \geqslant 0$, with the boundary conditions

$$\psi(x, 0) = 0, \qquad x < 0, \tag{2.27}$$

$$\left\{\left(\frac{d^2}{dx^2} - k^2\right)^2 - 1\right\}\eta(x) = -2i\tau\psi(x, 0), \quad x > 0. \tag{2.28}$$

The eigenvalue problem is now fully specified. Real positive values of k are sought that lead to non-trivial values of $\psi(x, z)$, $\eta(x)$, where $\psi(x, z)$ satisfies (2.16) in $z \geqslant 0$, (2.27) on $x < 0$, $z = 0$, and tends to zero as $|x^2 + z^2| \to \infty$, (2.10). Furthermore, $\eta(x)$ is given by (2.28), with edge constraints (2.24), (2.25) (in which $\eta(0)$ and $d\eta(0)/dx$ are bounded), and the displacement vanishes as $x \to \infty$. Finally, ψ and η are related by (2.26), and from this the edge constraints on η can easily be shown to enforce regular behaviour on ψ, namely:

$$\psi(x, z) = -i\left(z\eta(0) + xz\frac{d\eta}{dz}(0)\right) + o(|x^2 + z^2|), \quad |x^2 + z^2| \to 0. \tag{2.29}$$

3. Solution of the eigenvalue problem

(a) Wiener–Hopf analysis

The analysis begins by defining the half-range Fourier transforms of a function $\phi(x)$ as

$$\Phi^+(\alpha) = \int_0^\infty \phi(x)e^{i\alpha x}\,dx, \tag{3.1}$$

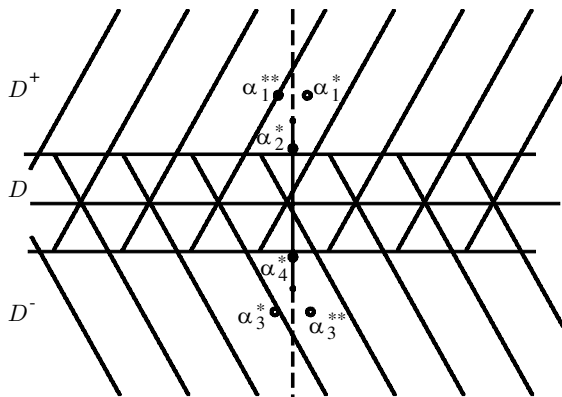$$\Phi^-(\alpha) = \int_{-\infty}^0 \phi(x)e^{i\alpha x}\,dx, \tag{3.2}$$

Figure 2. The complex α-plane showing the location of the branch points of $\gamma(\alpha)$ at $\pm i\sqrt{k^2 - k_0^2}$ (denoted by black dots), the direction of the branch cuts, and the zeros of $K(\alpha)$ at α_j^*, $j = 1, 2, 3, 4$ and α_k^{**}, $k = 1, 3$. The strip of analyticity in which the Wiener–Hopf equation (3.17) is defined is shown as $\mathcal{D}$, as well as the overlapping regions $\mathcal{D}^{\pm}$.

where $\Phi^+(\alpha) + \Phi^-(\alpha)$ is the usual full-range Fourier transform and α is a complex number in some region of the complex plane, usually containing the real line. The inverse is

$$\phi(x) = \frac{1}{2\pi} \int_{-\infty}^{\infty} [\Phi^+(\alpha) + \Phi^-(\alpha)] e^{-i\alpha x} \, d\alpha, \tag{3.3}$$

in which integration is along the real line in the complex α-plane. Of course, $\phi(x)$ must be such that the integrals exist, i.e. $\phi(x)$ tends to zero sufficiently rapidly as $x \to \infty$, and is integrable at the origin. The superscripts $+$ and $-$ in (3.1) and (3.2) denote the fact that such integrals (see Noble 1988) are analytic in the upper and lower halves of the α-plane, respectively, denoted by $\mathcal{D}^+$ and $\mathcal{D}^-$. These regions overlap in a strip, $\mathcal{D}$, enclosing the real line (as shown in figure 2). In what follows, k, k_0 and τ (or ϵ) are treated as fixed constants.

Applying a full-range Fourier transform to the governing equation (2.16), where

$$\Psi(\alpha, z) = \int_{-\infty}^{\infty} \psi(x, z) e^{i\alpha x} \, d\alpha, \quad \alpha \in \mathcal{D}, \tag{3.4}$$

and assuming the integrals thus obtained exist, gives

$$\frac{d^2\Psi}{dz^2}(\alpha, z) + (k_0^2 - k^2 - \alpha^2)\Psi(\alpha, z) = 0, \quad z \geqslant 0. \tag{3.5}$$

This is easily solved to yield

$$\Psi(\alpha, z) = A(\alpha) e^{-\gamma(\alpha)z} + B(\alpha) e^{\gamma(\alpha)z}, \tag{3.6}$$

where

$$\gamma(\alpha) = (\alpha^2 + k^2 - k_0^2)^{1/2} \tag{3.7}$$

is made a single-valued function of α by introducing branch cuts from $\pm i\infty$ to $\pm i(k^2 - k_0^2)^{1/2}$ in the upper/lower half-planes. Now, the branch points move onto the real

line if $k_0 \geqslant k$, which would negate the assumption in (3.3) that the inverse path can be taken along the real line. Indeed, as will be shown later, it is required that the finite width strip, $\mathcal{D}$ of figure 2, be free of singularities in order for a real eigenvalue k to exist. Therefore, one constraint is

$$k > k_0, \tag{3.8}$$

and if the Riemann surface of $\gamma(\alpha)$ is chosen such that

$$\gamma(0) = (k^2 - k_0^2)^{1/2}, \tag{3.9}$$

then the first term on the right-hand side of (3.6) tends to zero as $z \to \infty$ for each real α value, while the second term diverges. Thus, the requirement of vanishing ψ in the far-field yields

$$B(\alpha) \equiv 0, \tag{3.10}$$

and so, on $z = 0$, the relationship

$$\Psi^+(\alpha, 0) + \Psi^-(\alpha, 0) = \frac{-1}{\gamma(\alpha)}[\Psi_z^+(\alpha, 0) + \Psi_z^-(\alpha, 0)] = A(\alpha) \tag{3.11}$$

holds, in which the subscript denotes differentiation with respect to z.

Turning to the boundary conditions, equation (2.27) reveals that

$$\Psi^-(\alpha, 0) = 0, \tag{3.12}$$

whereas a half-range transform on (2.28), employing the edge constraints (2.24), (2.25), yields

$$[(\alpha^2 + k^2)^2 - 1]\Lambda^+(\alpha) = -2\mathrm{i}\tau\Psi^+(\alpha, 0) + [\mathrm{i}\alpha(\alpha^2 + (2-\nu)k^2)\eta_0 - (\alpha^2 + \nu k^2)\eta_1], \tag{3.13}$$

in which

$$\eta_0 = \eta(0), \qquad \eta_1 = \frac{\mathrm{d}\eta}{\mathrm{d}x}(0), \tag{3.14}$$

and

$$\Lambda^+(\alpha) = \int_0^\infty \eta(x)\mathrm{e}^{\mathrm{i}\alpha x}\,\mathrm{d}x. \tag{3.15}$$

From continuity of normal velocity, (2.26),

$$\Lambda^+(\alpha) = \mathrm{i}\Psi_z^+(\alpha, 0), \tag{3.16}$$

and so (3.13) and (3.12) may be employed to reduce the relationship (3.11) to one involving just $\Psi^+(\alpha, 0)$ and $\Psi_z^-(\alpha, 0)$:

$$\gamma(\alpha)K(\alpha)\Psi^+(\alpha, 0) = -\Psi_z^-(\alpha, 0)$$
$$- \frac{[\alpha(\alpha^2 + (2-\nu)k^2)\eta_0 + (\alpha^2 + \nu k^2)\mathrm{i}\eta_1]}{(\alpha^2 + k^2)^2 - 1}, \qquad \alpha \in \mathcal{D}. \tag{3.17}$$

This is the Wiener–Hopf functional equation, defined in a strip of finite width enclosing the real line of the α-plane, and

$$K(\alpha) = 1 - \frac{2\tau}{\gamma(\alpha)[(\alpha^2 + k^2)^2 - 1]}. \tag{3.18}$$

As mentioned above, the line of real α must be free of singularities. Therefore, $K(\alpha)$ must be zero and pole free for real α values. The denominator of the second term of $K(\alpha)$ has zeros at

$$\alpha_1 = \mathrm{i}(k^2 + 1)^{1/2}, \qquad \alpha_2 = \mathrm{i}(k^2 - 1)^{1/2}, \tag{3.19}$$

both of which lie in the upper half-plane if and only if

$$k > 1, \tag{3.20}$$

and, similarly, has zeros at

$$\alpha_3 = -\alpha_1 = -\mathrm{i}(k^2 + 1)^{1/2}, \qquad \alpha_4 = -\alpha_2 = -\mathrm{i}(k^2 - 1)^{1/2}, \tag{3.21}$$

in the lower half-plane. To ascertain the presence of zeros of $K(\alpha)$ on the real line, it is useful to look for intersections of the curve $(\alpha^2 + k^2)^2 - 1$ with $2\tau/\gamma(\alpha)$. The former is an even function that is strictly monotonic increasing in $\alpha \geqslant 0$, and, similarly, the latter is even and strictly monotonic decreasing in $\alpha \geqslant 0$ (recall that $k > k_0$ so that $\gamma(\alpha)$ is real and positive on $\mathrm{Im}(\alpha) = 0$). Thus, $K(\alpha)$ will not have a real zero if and only if

$$k^4 - 1 > \frac{2\tau}{\gamma(0)} = \frac{2\tau}{(k^2 - k_0^2)^{1/2}}, \tag{3.22}$$

and this gives a third (along with (3.8), (3.20)) constraint that k must satisfy. For convenience, let k_{f} denote the single positive zero of $K(0)$ (in terms of wavenumber k), that is, the fluid-loaded flexural wavenumber that exists at all frequencies and satisfies

$$k_{\mathrm{f}}^4 - 1 - \frac{2\epsilon}{k_0(k_{\mathrm{f}}^2 - k_0^2)^{1/2}} = 0, \quad k_{\mathrm{f}} > \max(1, k_0), \tag{3.23}$$

then the three constraints on k may be combined into the single one

$$k > k_{\mathrm{f}}. \tag{3.24}$$

For small τ and $k_0 < 1$, it is easily shown that $K(\alpha)$, with branch-cuts of $\gamma(\alpha)$ as shown in figure 2, has simple zeros at

$$\alpha_1^* \sim \alpha_1 + \frac{\tau}{2(k^2 + 1)^{1/2}(k_0^2 + 1)^{1/2}}, \tag{3.25}$$

$$\alpha_1^{**} \sim \alpha_1 - \frac{\tau}{2(k^2 + 1)^{1/2}(k_0^2 + 1)^{1/2}}, \tag{3.26}$$

$$\alpha_2^* \sim \alpha_2 - \frac{\mathrm{i}\tau}{2(k^2 - 1)^{1/2}(1 - k_0^2)^{1/2}} \tag{3.27}$$

in the upper half of the α-plane, and at

$$\alpha_3^* = -\alpha_1^*, \qquad \alpha_3^{**} = -\alpha_1^{**}, \qquad \alpha_4^* = -\alpha_2^* \tag{3.28}$$

in the lower half-plane. On the other Riemann sheet of the branch-cut function $\gamma(\alpha)$ there are four more zeros, making a total of ten, and these are located at α_2^{**}, $\alpha_4^{**} = -\alpha_2^{**}$, α_5^*, $\alpha_6^* = -\alpha_5^*$, where

$$\alpha_2^{**} \sim \alpha_2 + \frac{\mathrm{i}\tau}{2(k^2 - 1)^{1/2}(1 - k_0^2)^{1/2}}, \qquad k_0 < 1, \tag{3.29}$$

$$\alpha_5^* \sim \mathrm{i}\sqrt{k^2 - k_0^2} - \frac{2\tau^2\mathrm{i}}{(1 - k_0^4)^2\sqrt{k^2 - k_0^2}}, \qquad k_0 < 1. \tag{3.30}$$

As k_0 increases through the value unity, the picture changes somewhat. The zeros at α_1^*, α_1^{**}, plus their images at α_3^*, α_3^{**}, remain on the 'physical' Riemann surface, but the zeros ascribed the subscript 2 coalesce at $k_0 = 1$, and then *both* take locations on the 'non-physical' Riemann sheet. The latter is also true for the zeros with subscript 4. On the other hand, α_5^* and α_6^* also pass through the branch-point at $k_0 = 1$ but move *onto* the physical Riemann sheet when k_0 exceeds 1. For notational convenience it is appropriate to switch labels on α_2^* and α_5^* as they pass from/to the complex plane, respectively, as k_0 increases in value through unity. Hence, for small τ and $1 < k_0 < k$, the definition (3.27) is replaced by

$$\alpha_2^* \sim \mathrm{i}\sqrt{k^2 - k_0^2} - \frac{2\tau^2\mathrm{i}}{(k_0^4 - 1)^2\sqrt{k^2 - k_0^2}}, \tag{3.31}$$

and ditto for α_4^*.

The above asymptotic expressions (3.27), (3.31) for α_2^* are clearly invalid as k_0 approaches unity. For completeness, the asymptotic form valid in this vicinity is now given. Writing k_0 as

$$k_0^2 = 1 + \tau^{2/3}p, \quad p = \mathcal{O}(1), \quad \tau \to 0, \tag{3.32}$$

a little effort reveals that

$$\alpha_2^* \sim \mathrm{i}\sqrt{k^2 - 1 - \tau^{2/3}x}, \tag{3.33}$$

in which x is the real positive root of

$$x^3 - px^2 - 1 = 0. \tag{3.34}$$

Hence, at $k_0 = 1$, the quantity $p = 0$ and so $x = 1$, which gives

$$\alpha_2^* \sim \mathrm{i}\sqrt{k^2 - 1 - \tau^{2/3}}. \tag{3.35}$$

As $p \to -\infty$, that is the value of k_0 is below unity, the root of (3.34) behaves as

$$x \sim \sqrt{-1/p}, \tag{3.36}$$

which may be written, using (3.32), as

$$x \sim \tau^{1/3}/\sqrt{1 - k_0^2}. \tag{3.37}$$

Substituting this into (3.33) and expanding in τ recovers expression (3.27). Similarly, for $k_0 > 1$, the parameter p is taken to tend to $+\infty$, from which we deduce that the positive real root x (3.34) is

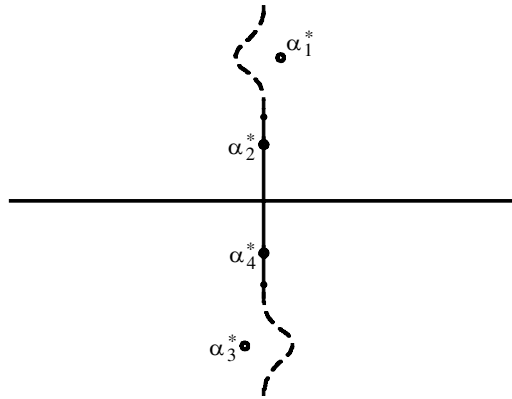$$x \sim p = (k_0^2 - 1)/\tau^{2/3}. \tag{3.38}$$

Figure 3. An indented choice of branch cuts that leads to just four zeros of $K(\alpha)$
on the chosen Riemann surface, at α_j^*, $j = 1, 2, 3, 4$.

Hence, in this limit, (3.33) yields

$$\alpha_2^* \sim i\sqrt{k^2 - k_0^2}, \tag{3.39}$$

which is the leading-order term in (3.31). The next order $(\mathcal{O}(\tau^2))$ could have been obtained by keeping higher-order terms in the root equation (3.34).

Note that, with the definitions employed above, α_2^* and its conjugate α_4^* *always* lie on the imaginary axis between branch points at $\pm i\sqrt{k^2 - k_0^2}$, for all $0 < k_0 < k$. Thus, if the branch cuts are indented, as shown in figure 3 (which puts the zeros α_1^{**}, α_3^{**} onto the other Riemann surface), then $K(\alpha)$ has exactly four zeros in the cut plane at the locations shown, α_i^*, $i = 1, 2, 3, 4$, $\forall \tau > 0$, $k > 1$, $0 < k_0 < k$. Note also in figure 2 how the strip $\mathcal{D}$ has width bounded by the points α_2^*, α_4^*.

It is now necessary to solve the Wiener–Hopf equation (3.17), and to achieve this (Noble 1988) it is necessary to decompose $K(\alpha)$ into the product

$$K(\alpha) = K^+(\alpha)K^-(\alpha), \tag{3.40}$$

where $K^+(\alpha)$ is free of singularities and zeros, and asymptotes to a constant as $|\alpha| \to \infty$, in $\mathcal{D}^+$ (see figure 2), whereas $K^-(\alpha)$ is free of singularities and zeros in $\mathcal{D}^-$ and tends to a constant value at infinity in this lower region. Without loss of generality, the relation

$$K^+(\alpha) = K^-(-\alpha), \quad \alpha \in \mathcal{D}^+, \tag{3.41}$$

can be imposed because $K(\alpha)$ is even in α, and using the standard product decomposition form (see, for example, Abrahams 1981),

$$K^\pm(\alpha) = \exp\left\{\frac{\pm 1}{2\pi i} \int_{-\infty}^\infty \frac{\log[K(\zeta)]}{\zeta - \alpha} \, d\zeta\right\} = \exp\left\{\frac{\pm \alpha}{\pi i} \int_0^\infty \frac{\log[K(\zeta)]}{\zeta^2 - \alpha^2} \, d\zeta\right\}, \tag{3.42}$$

in which α lies above the contour of integration for $K^+(\alpha)$ and below for $K^-(\alpha)$. If either factor is required on the real line, then the contour of the doubly infinite integral is deformed down for $K^+(\alpha)$ or indented upwards for $K^-(\alpha)$. Note that $\gamma(\alpha)$ was not incorporated in $K(\alpha)$ (i.e. in the coefficient multiplying Ψ^+ in (3.17)), because the present form of $K(\alpha)$ tends to unity as $\alpha \to \pm\infty$ in $\mathcal{D}$, hence ensuring

convergence of the integrals in (3.42). Thus, $\gamma(\alpha)$ must be factorized too, and this is achieved almost by inspection to yield (recalling the cut locations as shown in figure 2)

$$\gamma^{\pm}(\alpha) = (\alpha \pm i\sqrt{k^2 - k_0^2})^{1/2} e^{\mp i\pi/4}, \tag{3.43}$$

where the phase factors are added to ensure that

$$\gamma(\alpha) = \gamma^+(\alpha)\gamma^-(\alpha) \quad \text{and} \quad \gamma^+(\alpha) = \gamma^-(-\alpha). \tag{3.44}$$

Substituting (3.40) and (3.44) into (3.17) gives

$$\gamma^+(\alpha)K^+(\alpha)\Psi^+(\alpha, 0) = \frac{-1}{\gamma^-(\alpha)K^-(\alpha)}\Psi_z^-(\alpha, 0)$$
$$- \frac{[\alpha(\alpha^2 + (2-\nu)k^2)\eta_0 + (\alpha^2 + \nu k^2)i\eta_1]}{\gamma^-(\alpha)K^-(\alpha)[(\alpha^2 + k^2)^2 - 1]}, \quad \alpha \in \mathcal{D}, \tag{3.45}$$

which, by inspection, has a left-hand side free of singularities in the upper half-plane, $\mathcal{D}^+$. The right-hand side is free of singularities in the lower half-plane, $\mathcal{D}^-$, *except* for simple poles due to the denominator of the forcing term, i.e. $(\alpha^2 + k^2)^2 - 1 = 0$ or when $\alpha = \alpha_3 = -\alpha_1$, $\alpha = \alpha_4 = -\alpha_2$. These are easily moved to the left-hand side by the rearrangement

$$\gamma^+(\alpha)K^+(\alpha)\Psi^+(\alpha, 0) - \sum_{j=1}^{2} \frac{f(\alpha_j)\eta_0 + g(\alpha_j)\eta_1}{\alpha + \alpha_j}$$
$$= \frac{-1}{\gamma^-(\alpha)K^-(\alpha)}\Psi_z^-(\alpha, 0) - \frac{[\alpha(\alpha^2 + (2-\nu)k^2)\eta_0 + (\alpha^2 + \nu k^2)i\eta_1]}{\gamma^-(\alpha)K^-(\alpha)[(\alpha^2 + k^2)^2 - 1]}$$
$$- \sum_{j=1}^{2} \frac{f(\alpha_j)\eta_0 + g(\alpha_j)\eta_1}{\alpha + \alpha_j}, \tag{3.46}$$

where

$$f(\alpha) = \frac{-(\alpha^2 + (2-\nu)k^2)}{4\gamma^+(\alpha)K^+(\alpha)(\alpha^2 + k^2)}, \qquad g(\alpha) = \frac{i(\alpha^2 + \nu k^2)}{4\gamma^+(\alpha)K^+(\alpha)\alpha(\alpha^2 + k^2)} \tag{3.47}$$

are chosen in order to suppress the two poles in the lower half-plane on the right-hand side. Note that in the above expressions, the relations (3.41), (3.44), etc., have been employed so as to work in terms of α_1^*, α_2^*, rather than α_3^* and α_4^*. So, the left-hand side of (3.46) is now analytic in $\mathcal{D}^+$ and the right-hand side is analytic in $\mathcal{D}^-$, and, hence, both sides give analytic continuations of α from $\mathcal{D}$ into the whole complex plane. Therefore, both sides are equal to an entire function, $E(\alpha)$ say. To determine this function, it is necessary to examine the large asymptotic behaviour of both sides of (3.46) in their respective half-planes of analyticity. First, $K^{\pm}(\alpha)$ tend to unity and $\gamma^{\pm}(\alpha) = \mathcal{O}(\alpha^{1/2})$ as $|\alpha| \to \infty$ in $\mathcal{D}^{\pm}$ by observation of (3.42), (3.43). Second, the local behaviour of $\psi(x, z)$ around the edge of the plate (2.29) determines the large-$|\alpha|$ behaviour of $\Psi^+(\alpha, 0)$, $\Psi_z^-(\alpha, 0)$. From the relations discussed in eqn (1.74) of Noble (1988) it is deduced that

$$\Psi^+(\alpha, 0) = o(\alpha^{-2}), \quad |\alpha| \to \infty, \quad \alpha \in \mathcal{D}^+, \tag{3.48}$$
$$\Psi_z^-(\alpha, 0) = \mathcal{O}(\alpha^{-1}), \quad |\alpha| \to \infty, \quad \alpha \in \mathcal{D}^-. \tag{3.49}$$

Therefore, both sides of equation (3.46) tend to zero in respective overlapping half-planes, and, by invoking Liouville's theorem, it is found that the entire function $E(\alpha) \equiv 0$.

The solution of the eigen-boundary-value problem is now obtained from

$$A(\alpha) = \Psi(\alpha,0) = \Psi^+(\alpha,0) = \frac{1}{\gamma^+(\alpha)K^+(\alpha)} \sum_{j=1}^{2} \frac{f(\alpha_j)\eta_0 + g(\alpha_j)\eta_1}{\alpha + \alpha_j}, \qquad (3.50)$$

by employing (3.6), (3.10) and the inverse Fourier transform

$$\psi(x,z) = \frac{1}{2\pi} \int_{-\infty}^{\infty} \Psi(\alpha,0) e^{-i\alpha x - \gamma(\alpha)z} \, d\alpha. \qquad (3.51)$$

This form (3.50) is suitable for the region $x < 0$, where deformation of the integration path into the upper half-plane, wrapping the contour around the upper branch cut, is expedient. For $x > 0$ it is more useful to employ the expression

$$\Psi(\alpha,0) = A(\alpha) = \frac{\gamma^-(\alpha)K^-(\alpha)[(\alpha^2+k^2)^2-1]}{\{[(\alpha^2+k^2)^2-1]\gamma(\alpha)-2\tau\}} \sum_{j=1}^{2} \frac{f(\alpha_j)\eta_0 + g(\alpha_j)\eta_1}{\alpha + \alpha_j}, \qquad (3.52)$$

where the singularities in the lower half-plane can now be seen explicitly in the denominator, i.e. a branch cut of $\gamma(\alpha)$ in the lower half-plane and simple poles at $\alpha = \alpha_3^*, \alpha_4^*$ (and α_3^{**} if the cut is not indented). From this, and (2.26), it is easily deduced that the plate displacement is given by

$$\eta(x) = \frac{-i}{2\pi} \int_{-\infty}^{\infty} \gamma(\alpha)\Psi(\alpha,0) e^{-i\alpha x} \, d\alpha, \quad x > 0. \qquad (3.53)$$

(b) The edge-wave dispersion relation

The final matter to attend to is to establish the values of k for which the above solutions are valid. So far, the only restrictions on k are those given by (3.8), (3.20) and (3.22), but are there any other requirements which have not, as yet, been satisfied? Well, an issue that remains to be checked is the requirement that $\Lambda^+(\alpha)$, the half-range Fourier transform of $\eta(x)$ (3.15), is analytic in $\mathcal{D}^+$. The value of this can be determined explicitly from relation (3.13),

$$\Lambda^+(\alpha) = \frac{-2i\tau\Psi^+(\alpha,0) + [i\alpha(\alpha^2+(2-\nu)k^2)\eta_0 - (\alpha^2+\nu k^2)\eta_1]}{\{(\alpha^2+k^2)^2-1\}}, \qquad (3.54)$$

where $\Psi^+(\alpha,0)$ is known from (3.50). As is apparent, this has poles in the upper half-plane, $\mathcal{D}$, at $\alpha = \alpha_1, \alpha_2$ unless the numerator is *chosen* to vanish at these points. This gives the two conditions

$$\alpha_j(\alpha_j^2 + (2-\nu)k^2)\eta_0 + (\alpha_j^2 + \nu k^2)i\eta_1 = 2\tau\Psi^+(\alpha_j,0), \quad j = 1,2, \qquad (3.55)$$

which may be written in terms of the quantities, $f(\alpha), g(\alpha)$, given in (3.47):

$$-f(\alpha_j)\eta_0 + g(\alpha_j)\eta_1 = \frac{\tau[\gamma^+(\alpha_j)K^+(\alpha_j)]^{-2}}{2\alpha_j(\alpha_j^2+k^2)} \sum_{k=1}^{2} \frac{f(\alpha_k)\eta_0 + g(\alpha_k)\eta_1}{\alpha_j + \alpha_k}, \quad j = 1,2. \qquad (3.56)$$

Hence, if

$$h(\alpha) = \frac{\tau}{2\alpha(\alpha^2 + k^2)[\gamma^+(\alpha)K^+(\alpha)]^2}, \tag{3.57}$$

then a further simplification yields the matrix form:

$$\begin{bmatrix} \dfrac{h(\alpha_1)f(\alpha_1)}{2\alpha_1} + \dfrac{h(\alpha_1)f(\alpha_2)}{\alpha_1 + \alpha_2} + f(\alpha_1) & \dfrac{h(\alpha_1)g(\alpha_1)}{2\alpha_1} + \dfrac{h(\alpha_1)g(\alpha_2)}{\alpha_1 + \alpha_2} - g(\alpha_1) \\[2ex] \dfrac{h(\alpha_2)f(\alpha_1)}{\alpha_1 + \alpha_2} + \dfrac{h(\alpha_2)f(\alpha_2)}{2\alpha_2} + f(\alpha_2) & \dfrac{h(\alpha_2)g(\alpha_1)}{\alpha_1 + \alpha_2} + \dfrac{h(\alpha_2)g(\alpha_2)}{2\alpha_2} - g(\alpha_2) \end{bmatrix} \begin{pmatrix} \eta_0 \\ \eta_1 \end{pmatrix}$$

$$= \begin{pmatrix} 0 \\ 0 \end{pmatrix}. \tag{3.58}$$

Clearly, this system has a non-trivial solution if and only if

$$\left[\frac{[h(\alpha_1) + 2\alpha_1]f(\alpha_1)}{2\alpha_1} + \frac{h(\alpha_1)f(\alpha_2)}{\alpha_1 + \alpha_2} \right]\left[\frac{h(\alpha_2)g(\alpha_1)}{\alpha_1 + \alpha_2} + \frac{[h(\alpha_2) - 2\alpha_2]g(\alpha_2)}{2\alpha_2} \right]$$
$$- \left[\frac{[h(\alpha_1) - 2\alpha_1]g(\alpha_1)}{2\alpha_1} + \frac{h(\alpha_1)g(\alpha_2)}{\alpha_1 + \alpha_2} \right]\left[\frac{h(\alpha_2)f(\alpha_1)}{\alpha_1 + \alpha_2} + \frac{[h(\alpha_2) + 2\alpha_2]f(\alpha_2)}{2\alpha_2} \right] = 0, \tag{3.59}$$

and then the edge constants may be expressed as

$$\eta(0) = \eta_0 = \left\{ \frac{[h(\alpha_1) - 2\alpha_1]g(\alpha_1)}{2\alpha_1} + \frac{h(\alpha_1)g(\alpha_2)}{\alpha_1 + \alpha_2} \right\} C, \tag{3.60}$$

$$\frac{d\eta}{dx}(0) = \eta_1 = -\left\{ \frac{[h(\alpha_1) + 2\alpha_1]f(\alpha_1)}{2\alpha_1} + \frac{h(\alpha_1)f(\alpha_2)}{\alpha_1 + \alpha_2} \right\} C, \tag{3.61}$$

in terms of an arbitrary parameter C. Equation (3.59) is a dispersion relation from which is deduced the real positive value of k, should one or more exist, for given values of k_0 and τ. The solution of the eigenvalue-Wiener–Hopf problem is now complete. Should a real value of k satisfy (3.59), then there is a non-trivial non-attenuating fluid-coupled plate wave (2.14), (2.15) with cross-sectional form given by (3.51), (3.53) and (3.50). The following section examines a few features of this cross-sectional behaviour of the edge wave, i.e. $\psi(x,z)$ and $\eta(x)$, and the solution (3.59) is the subject of discussion in § 5.

4. The wave field far from the plate edge

For completeness, the field of the edge wave far from the edge will now be determined, including the form of the plate deflection as $x \to \infty$. To do this, it is convenient to deform the Fourier inverse integral contour of the integral representation of $\psi(x,z)$ in (3.51), that is,

$$\psi(x,z) = \frac{1}{2\pi} \int_{-\infty}^{\infty} \Psi(\alpha, 0)e^{-i\alpha x - \gamma(\alpha)z} \, d\alpha, \tag{4.1}$$

into its steepest-descent path. It is taken here that a real edge-wave wavenumber k, satisfying (3.59), exists for a given set of dimensionless parameters ν, k_0 and τ (see

(2.11), (2.17) and (2.19) for their relation to the physical quantities describing the plate and fluid). So, the inverse path, originally along the real line, is deformed up or down for $x < 0$ or $x > 0$, respectively. In particular, the steepest-descent path will easily be deduced after making the transformation

$$\alpha = -\mathrm{i}\sqrt{k^2 - k_0^2}\cos\zeta, \tag{4.2}$$

in which ζ is chosen to traverse the path $\mathrm{i}\infty + \pi/2$ to $-\mathrm{i}\infty + \pi/2$ as α goes from $-\infty$ to ∞. With this branch then

$$\gamma(\alpha) = \sqrt{k^2 - k_0^2}\sin\zeta, \tag{4.3}$$

in order to satisfy the Riemann sheet requirement that $\gamma(0) = \sqrt{k^2 - k_0^2}$ at $\zeta = \pi/2$. Writing the physical variables in polar form,

$$x = r\cos\theta, \quad z = r\sin\theta, \quad 0 \leqslant \theta \leqslant \pi, \tag{4.4}$$

allows the exponent in the integrand of (3.51) to be expressed as

$$-\mathrm{i}\alpha x - \gamma(\alpha)z = -r\sqrt{k^2 - k_0^2}\cos(\zeta - \theta), \tag{4.5}$$

and, clearly, the steepest-descent path as $r \to \infty$ (fixed $\sqrt{k^2 - k_0^2}$) lies along the contour $+\mathrm{i}\infty + \theta \to \zeta \to -\mathrm{i}\infty + \theta$, which, in the α-plane, is a hyperbolic path with turning point at $\alpha = -\mathrm{i}\sqrt{k^2 - k_0^2}\cos\theta$ and asymptotes $\mp\theta - \pi/2$.

For $\theta > \pi/2$, or $x < 0$, deformation of the integral contour into a hyperbolic path in the upper half of the α-plane can be performed without crossing any singularities of $\Psi(\alpha, 0)$, because this is equivalent to $\Psi^+(\alpha, 0)$ (3.50). Standard steepest-descent analysis yields

$$\psi(x, z) \sim \frac{(k^2 - k_0^2)^{1/4}}{\sqrt{2\pi r}}\sin\theta\,\Psi(-\mathrm{i}\sqrt{k^2 - k_0^2}\cos\theta, 0)\mathrm{e}^{-r\sqrt{k^2 - k_0^2}\cos\theta}, \tag{4.6}$$

for $\theta > \pi/2$, where $\Psi(\alpha, 0)$ is written in (3.50). When $\theta < \pi/2$, this expression (4.6) is still valid, with $\Psi(\alpha, 0)$,

$$\alpha = -\mathrm{i}\sqrt{k^2 - k_0^2}\cos\theta,$$

deduced from (3.52) as long as no singularities are crossed in the contour deformation. As θ is decreased to 0, the steepest-descent contour is wrapped closer and closer around the lower branch cut, and will eventually cross first one and then another of the poles of $\Psi(\alpha, 0)$ arising from the zeros of $K(\alpha)$. The pole at α_4^* (see (3.28) and figure 2) lies between 0 and $-\mathrm{i}\sqrt{k^2 - k_0^2}$ and will contribute to $\psi(x, z)$ when

$$\sqrt{k^2 - k_0^2}\cos\theta > +\mathrm{i}\alpha_4^* = -\mathrm{i}\alpha_2^* \tag{4.7}$$

or

$$\theta < \cos^{-1}\left(\frac{\mathrm{i}\alpha_4^*}{\sqrt{k^2 - k_0^2}}\right) = \theta_4. \tag{4.8}$$

Similarly, the two roots at α_3^*, α_3^{**} contribute if they are passed during deformation, and this occurs if and only if

$$\theta < \mathrm{Re}\left[\cos^{-1}\left(\frac{\mathrm{i}\alpha_3^*}{\sqrt{k^2 - k_0^2}}\right)\right] = \theta_3, \tag{4.9}$$

i.e. the images of α_3^*, α_3^{**} in the ζ-plane lie to the right of the line $\mathrm{Re}(\zeta) = \theta$. It is a straightforward matter to deduce the residue at both these pole locations, and so, omitting this detail, the expression for the far-field form of $\psi(x,z)$ in $0 < \theta \leqslant \pi/2$ is

$$\psi(x,z) \sim \frac{(k^2 - k_0^2)^{1/4}}{\sqrt{2\pi r}} \sin\theta \Psi(-\mathrm{i}\sqrt{k^2 - k_0^2}\cos\theta, 0)\mathrm{e}^{-r\sqrt{k^2 - k_0^2}\cos\theta}$$
$$- \mathrm{i}A_4^* \, \mathrm{H}(\theta_4 - \theta)\mathrm{e}^{-r\sqrt{k^2 - k_0^2}\cos(\theta_4 - \theta)}$$
$$- \mathrm{i}A_3^* \, \mathrm{H}(\theta_3 - \theta)\mathrm{e}^{-r\sqrt{k^2 - k_0^2}\cos(\theta_3^* - \theta)}$$
$$- \mathrm{i}A_3^{**} \, \mathrm{H}(\theta_3 - \theta)\mathrm{e}^{-r\sqrt{k^2 - k_0^2}\cos(\theta_3^{**} - \theta)}, \tag{4.10}$$

as $r \to \infty$, in which $\mathrm{H}(x)$ is the Heaviside function. Here, A_4^*, etc., are defined by

$$A_4^* = \lim_{\alpha \to \alpha_4^*} \{(\alpha - \alpha_4^*)\Psi(\alpha, 0)\}, \tag{4.11}$$

$$A_3^* = \lim_{\alpha \to \alpha_3^*} \{(\alpha - \alpha_3^*)\Psi(\alpha, 0)\}, \qquad A_3^{**} = \lim_{\alpha \to \alpha_3^{**}} \{(\alpha - \alpha_3^{**})\Psi(\alpha, 0)\}, \tag{4.12}$$

and

$$\cos\theta_3^* = \frac{\mathrm{i}\alpha_3^*}{\sqrt{k^2 - k_0^2}}, \qquad \cos\theta_3^{**} = \frac{\mathrm{i}\alpha_3^{**}}{\sqrt{k^2 - k_0^2}}. \tag{4.13}$$

Note that this asymptotic result is not valid for observation angles, θ, close to θ_3, θ_4. At these values the integrals have a pole in the vicinity of the saddle point, and so a uniform result over all $\pi < \theta < 0$ can be obtained, if required, via the use of Fresnel integrals (Noble 1988). As we do not use (4.10) further in this article, it is not necessary to perform this operation here.

The final issue for this section is to estimate the deflection of the plate far from the edge. For this, the integral expression (3.53) is employed after deformation into its steepest-descent path. This path, consistent with what is discussed above when $\theta = 0$, starts at $-\mathrm{i}\infty$, passes along the left-hand side of the lower branch cut (figure 2), around the branch point, and then to $-\mathrm{i}\infty$ on the right-hand side of the cut. As found for $\psi(x,z)$ for small enough θ, the poles at α_4^*, α_3^*, α_3^{**} are crossed during deformation, and will therefore contribute towards the total deflection $\eta(x)$. Just for the moment, taking the steepest-descent integral contribution of $\eta(x)$, called $\hat{\eta}(x)$ say, and applying transformation (4.2), yields

$$\hat{\eta}(x) = \frac{-(k^2 - k_0^2)}{2\pi} \int_{-\mathrm{i}\infty}^{\mathrm{i}\infty} \sin^2\zeta \Psi(-\mathrm{i}\sqrt{k^2 - k_0^2}\cos\zeta, 0)\mathrm{e}^{-x\sqrt{k^2 - k_0^2}\cos\zeta} \, \mathrm{d}\zeta. \tag{4.14}$$

The dominant contribution from the integrand comes from near $\zeta = 0$ for large x, and so

$$\hat{\eta}(x) \sim \frac{\mathrm{i}(k^2 - k_0^2)}{2\pi}\Psi(-\mathrm{i}\sqrt{k^2 - k_0^2}, 0)\mathrm{e}^{-x\sqrt{k^2 - k_0^2}} \int_{-\infty}^{\infty} v^2 \mathrm{e}^{-x\sqrt{k^2 - k_0^2}v^2/2} \, \mathrm{d}v, \tag{4.15}$$

or, on evaluation,

$$\hat{\eta}(x) \sim \frac{\mathrm{i}(k^2 - k_0^2)^{1/4}}{\sqrt{2\pi x^3}}\Psi(-\mathrm{i}\sqrt{k^2 - k_0^2}, 0)\mathrm{e}^{-x\sqrt{k^2 - k_0^2}}, \qquad x \to \infty. \tag{4.16}$$

The residue terms at α_3^*, α_3^{**}, α_4^* must be added to this in order to obtain the full displacement term. After some algebra it is found that

$$\eta(x) \sim \hat{\eta}(x) - A_4^* \sqrt{k^2 - k_0^2} \sin\theta_4 e^{-x\sqrt{k^2 - k_0^2}\cos\theta_4}$$
$$- A_3^* \sqrt{k^2 - k_0^2} \sin\theta_3^* e^{-x\sqrt{k^2 - k_0^2}\cos\theta_3^*}$$
$$- A_3^{**} \sqrt{k^2 - k_0^2} \sin\theta_3^{**} e^{-x\sqrt{k^2 - k_0^2}\cos\theta_3^{**}}, \quad x \to \infty, \tag{4.17}$$

where A_3^*, etc., are given in (4.11), (4.12).

The far-field fluid potential and plate displacement terms, as can be seen from (4.10), contain exponentially decaying contributions as long as θ_4 and the real part of θ_3^* (or θ_3^{**}, which is its complex conjugate) lie between 0 and $\pi/2$. This is indeed the case in view of discussions regarding α_3^*, etc., in § 3. The first term in (4.10) has a further decay factor $\mathcal{O}(r^{-1/2})$, which is due to cylindrical spreading of this edge-wave contribution, and its counterpart in the plate deflection, namely $\hat{\eta}(x)$, has a more rapid algebraic decay factor $\mathcal{O}(x^{-3/2})$. The pair of terms resulting from the zeros at α_3^*, α_3^{**} have exponents that are complex. Therefore, they oscillate with radial distance, r, as well as decaying. This is of no consequence as $\psi(x, z)$ and $\eta(x)$ still decay to 0 as $(x^2 + y^2)^{1/2} \to \infty$, as expected. In conclusion, if the integral expressions of $\psi(x, z)$, $\eta(x)$ ((3.51) and (3.53)) are free of zeros on the real line, then they decay to 0 in all directions away from the edge. Therefore, all the energy of the edge wave is confined to the vicinity of the edge and propagates along the edge, in the y-direction.

5. Existence of real eigen-wavenumbers

(a) The dispersion relation for k

Substantial, but straightforward, manipulation allows the full dispersion relation (3.59) to be written in the simplified form

$$\left(1 + \frac{\epsilon^2}{4(\sqrt{k^2+1}+\sqrt{k^2-1})^4 K_1^2 K_2^2}\right)\left(\frac{r_+^2(k)}{\sqrt{k^2+1}} - \frac{r_-^2(k)}{\sqrt{k^2-1}}\right)$$
$$= \tfrac{1}{4}\epsilon\left(\frac{1}{K_1^2} + \frac{1}{K_2^2}\right)\left(\frac{r_+^2(k)}{\sqrt{k^2+1}} + \frac{r_-^2(k)}{\sqrt{k^2-1}}\right) + \frac{2\epsilon r_+(k)r_-(k)}{K_1 K_2(\sqrt{k^2+1}+\sqrt{k^2-1})}, \tag{5.1}$$

where

$$K_1 = \sqrt{k^2+1}k_0^{1/2}(\sqrt{k^2+1}+\sqrt{k^2-k_0^2})^{1/2}K^+(\alpha_1), \tag{5.2}$$

$$K_2 = \sqrt{k^2-1}k_0^{1/2}(\sqrt{k^2-1}+\sqrt{k^2-k_0^2})^{1/2}K^+(\alpha_2), \tag{5.3}$$

and

$$r_\pm(k) = 1 \pm (1-\nu)k^2. \tag{5.4}$$

It should be stressed that expression (5.1) is exact and so holds for all values of the plate and fluid parameters, i.e. ϵ (or τ), ν and k_0.

The first point to ensure is that the dispersion relation (5.1) reduces to that for the *in vacuo* plate edge wave when fluid loading, ϵ, vanishes. Setting $\epsilon = 0$ in (5.1) yields

$$\frac{(1+(1-\nu)k^2)^2}{\sqrt{k^2+1}} = \frac{(1-(1-\nu)k^2)^2}{\sqrt{k^2-1}}. \tag{5.5}$$

This has a *single positive root* for $0 < \nu < 1/2$ at $k = k_v$, where

$$k_v = \left(\frac{1 - 3\nu + 2(1 - 2\nu + 2\nu^2)^{1/2}}{(3 + \nu)(1 - \nu)^2} \right)^{1/4}, \tag{5.6}$$

in agreement with the value found previously by Konenkov (1960) and by Thurston & McKenna (1974). In this case, the plate deflection is given by (from (3.53)) the integral

$$\eta(x) = \frac{-\mathrm{i}}{2\pi} \int_{-\infty}^{\infty} \gamma^-(\alpha) \sum_{j=1}^{2} \frac{(f(\alpha_j)\eta_0 + g(\alpha_j)\eta_1)}{\alpha + \alpha_j} \mathrm{e}^{-\mathrm{i}\alpha x} \, \mathrm{d}\alpha, \tag{5.7}$$

which can be determined explicitly as

$$\eta(x) = \frac{\eta_0}{2}\{(1 - (1 - \nu)k^2)\mathrm{e}^{-x\sqrt{k^2+1}} + (1 + (1 - \nu)k^2)\mathrm{e}^{-x\sqrt{k^2-1}}\}, \tag{5.8}$$

and the relationships (3.60) and (3.61) reduce to

$$\eta_1 = -(k^4 - 1)^{1/4}\eta_0, \tag{5.9}$$

after employing the dispersion relation (5.5).

The question may be asked: are there any real values of k that satisfy (5.1) for non-zero ϵ? Indeed, perhaps there always exists such a root for all ϵ, as is found to be the case for the usual fluid-loaded flexural wave k_f that solves (3.23) (Abrahams 1981). To disprove the latter suggestion, it is possible to reduce (5.1) to a simple form when $\epsilon \to \infty$. From the definition of the kernel functions (3.18), clearly

$$K(\alpha) \sim \frac{-2\epsilon}{\gamma(\alpha)k_0[(\alpha^2 + k^2)^2 - 1]}, \quad \epsilon \to \infty, \tag{5.10}$$

for fixed α, and so

$$K^+(\alpha) \sim \frac{\sqrt{2\epsilon}\mathrm{i}}{\gamma^+(\alpha)(\alpha + \alpha_1)(\alpha + \alpha_2)k_0^{1/2}} \tag{5.11}$$

in a bounded region of $\mathcal{D}^+$. Hence, substituting this into (5.2), (5.3) and (5.4) yields

$$K_1 \sim K_2 \sim \frac{-\mathrm{i}\sqrt{\epsilon/(2k_0)}}{\sqrt{k^2 + 1} + \sqrt{k^2 - 1}}, \tag{5.12}$$

which simplifies (5.1) down to

$$8(\sqrt{k^2 + 1} + \sqrt{k^2 - 1}) = 0. \tag{5.13}$$

Note that this relation is not only independent of ϵ, as it should of course be, but also free of k_0 and ν. It only involves the wavenumber k, and it is clear that no real roots $(k > 1)$ of this equation exist.

To summarize: for $\epsilon = 0$ there is a unique real k root of the dispersion relation, but no such root exists when $\epsilon \to \infty$. Therefore, it seems likely that a window of values of ϵ around $\epsilon = 0$ yields a real edge-wave wavenumber. Without significant effort it appears that little progress can be made analytically to deduce the roots of this equation, except under these limiting cases of zero fluid loading, and asymptotically as the fluid loading becomes very large. We turn, therefore, to numerical 'experimentation' to elucidate the existence of roots under finite fluid loading.
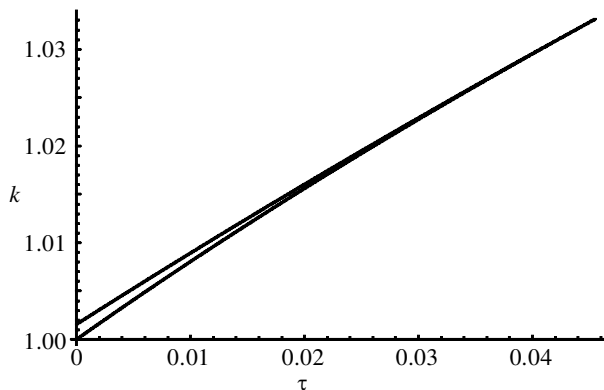
Figure 4. Plot of edge-wave wavenumber, k (i.e. the positive real root of the dispersion relation (5.1)), against $\tau = \epsilon/k_0$ for values of the dimensionless fluid wavenumber $k_0 = 0.8$ (2.17) and Poisson's ratio $\nu = 0.334$. The upper curve is the wavenumber solution k and the lower curve is k_{f}.

(b) Numerical solution and discussion

It is a simple enough matter to evaluate (5.1) numerically for given ϵ and k_0, and then march through real k values satisfying (3.24) to see if it vanishes. Note that all terms in the above relation contain even powers of k (as indeed they must from symmetry in y), and so if a positive root of (3.59) is found, then there is a corresponding root at $-k$.

Numerical studies reveal that for each value of ν ($0 < \nu < 0.5$) and k_0 ($k_0 < 1$) there is a *finite range of values, from zero up to some maximum, of* ϵ that permit real k solutions of (5.1). In practice it is found that such ϵ values are always small; for example, figure 4 illustrates the real edge-wave wavenumbers, k, for $k_0 = 0.8$, $\nu = 0.334$ against $\tau = \epsilon/k_0$. The top curve is that for k, and the bottom curve is k_{f}, the plate fluid-loaded wavenumber. As discussed in § 3, the wavenumber root k must lie above k_{f}, otherwise no unattenuated edge waves can exist. Clearly, as ϵ increases, the two curves converge and meet at around $\epsilon \approx 0.0363$. This is the fluid-loading value above which real edge-wave wavenumbers cannot exist. Figure 4 is typical of the variations of k with ϵ found for all k_0 (< 1), ν values.

Note, when $k_0 > 1$, numerical experiment reveals a small window of values that allow real k. These real k roots occur for k_0 very slightly above unity and for remarkably small fluid loading ϵ. For example, $k_0 = 1.001$ and $\epsilon = 0.000\,01$ yields a k value between 1.0015 and 1.0016. As k_0 increases further, the maximum ϵ decreases rapidly. The authors have found few parameter values of physical relevance (one such is discussed below) that fit into this small window. It is concluded that, while it may be viewed as somewhat surprising to find that an unattenuated edge wave can exist which propagates in a system, and at a frequency, at which flexural waves would be supersonic (although the edge wave itself is still subsonic), this is not found to be of great practical significance in everyday applications.

Having established that edge waves can propagate without energy loss along the free edge of a thin elastic plate immersed in an inviscid fluid, it is important to check on the physical relevance of such a result. To do this, three plates of differing material properties are examined. The properties of the three materials are listed in table 1.

Table 1. *Plate material parameters*

(The values for brass and Plexiglas are taken from Krylov (1998). This article provides the longitudinal and shear wave speeds, C_l and C_t, respectively, in terms of which $\nu = 0.5 + 0.5/(1 - C_l^2/C_t^2)$ and $E = 2(1 + \nu)\rho_p C_t^2$.)

	aluminium	brass	Plexiglas
ρ_p (10^3 kg m^{-3})	2.80	8.60	1.18
E (10^{10} N m^{-2})	7.40	10.45	0.585
ν	0.330	0.343	0.334

Table 2. *The non-dimensional fluid-loading parameter ϵ*

	aluminium	brass	Plexiglas
air	0.0020	0.0005	0.0021
water	0.3902	0.0866	0.4016

Table 3. *Coincidence frequency*

(The coincidence frequency $f_c = \omega_c/(2\pi)$ (Hz) for a plate of thickness 1 cm.)

	aluminium	brass	Plexiglas
air	1 103	1 618	2 541
water	20 963	30 766	48 324

Two fluids are considered, with typical ambient densities and sound speeds:

$$\text{air,} \qquad \rho_f = 1.2 \text{ kg m}^{-3}, \qquad c = 330 \text{ m s}^{-1}; \tag{5.14}$$

$$\text{water,} \quad \rho_f = 1000 \text{ kg m}^{-3}, \quad c = 1439 \text{ m s}^{-1}. \tag{5.15}$$

The values of the fluid-loading parameter ϵ are listed in table 2 for the various combinations of solid and fluid. We consider the three plate materials in turn.

For aluminium plates the values of the fluid-loading parameter ϵ given in table 2 are quite disparate for air and water, 0.002 and 0.392, respectively. The associated values of the coincidence frequency f_c for plates of thickness $h = 1$ cm are given in table 3. The coincidence frequency is inversely proportional to thickness, see (2.23), and $k_0 = \sqrt{f/f_c}$, where $f = \omega/(2\pi)$ is the frequency of the waves in cycles per second (Hz). Hence, the dimensionless quantity k_0 depends upon frequency and plate thickness as

$$k_0 \approx (fh)^{1/2} \times \begin{cases} 0.301\,17, & \text{for aluminium in air,} \\ 0.069\,07, & \text{for aluminium in water,} \end{cases} \tag{5.16}$$

where $f \times h$ is the frequency of vibration times plate thickness, measured in metres per second. It transpires that this value of k_0 for aluminium in air (with $\epsilon = 0.002$) yields a real root of (5.1) for all $f \times h$ between about 0.004 m s^{-1} and 10.95 m s^{-1}. That is, for a plate of thickness, h, say 2.5 mm, greater than a frequency of 1.6 Hz
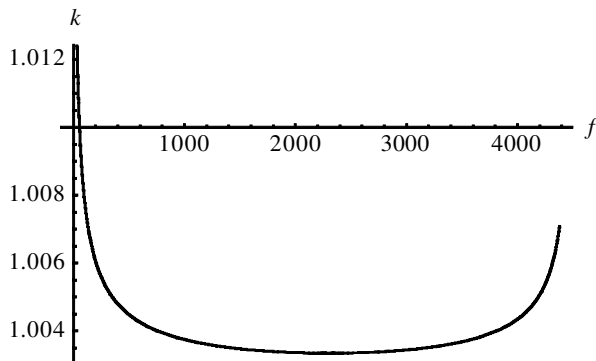
Figure 5. Plot of the real wavenumber, k, versus frequency, f,
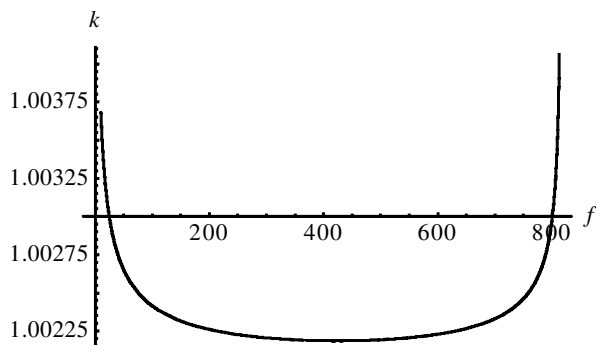for an aluminium plate in air with $h = 2.5$ mm.

Figure 6. Plot of the real wavenumber, k, versus frequency, f, for a brass plate in air with $h = 2$ cm. Note that 809 Hz is the coincidence frequency at which the fluid wavenumber equals the wavenumber flexural waves on the plate *in vacuo*.

and less than 4380 Hz, as shown in figure 5. Note that, for this thickness of plate, coincidence frequency in air occurs at $f_c \approx 4410$ Hz. It is also worth remarking that it is unclear from figure 5 that the lower bound on frequency is a positive number *greater* than zero. The asymptote of the curve looks like it could tend to the abscissa! However, a non-zero lower bound is confirmed in later discussion (see figure 7). Note that the above results are not the same for underwater situations. Then, no real roots of the dispersion relation (5.1) can be found for this set of parameters for any choice of $f \times h$. As discussed above, if the fluid loading is too large, then the edge-wave mode is cut off, and this is found to be true in this case.

Turning to brass plates, it is found that

$$k_0 \approx (fh)^{1/2} \times \begin{cases} 0.248\,61, & \text{in air,} \\ 0.057\,01, & \text{in water.} \end{cases} \tag{5.17}$$

Once again, no unattenuated edge waves exist for a brass plate in water. However, for air, the edge wave propagates without loss as long as $f \times h$ lies between about $0.000\,26$ m s^{-1} and 16.26 m s^{-1}, which corresponds to $f \approx 0.013$–813 Hz for a 2 cm thick plate. The plot of k versus f is given in figure 6 for this value of h. Note that the coincidence frequency occurs at $f_c \approx 809$ Hz for $h = 2$ cm, and so figure 6
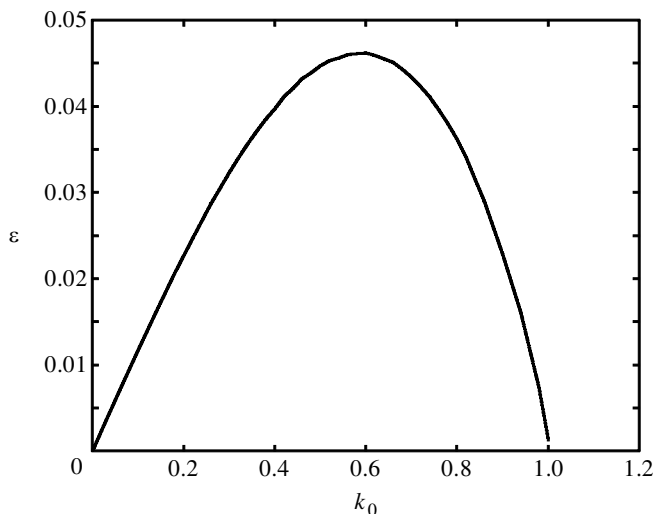
Figure 7. The maximum possible value of fluid loading, ϵ, as a function of frequency, k_0, for $\nu = 0.33$. Alternatively, for each ϵ, the edge wave cuts off at the frequencies indicated by the curve.

demonstrates that real k eigenvalues occur at values of k_0 marginally greater than unity. This is not commonly found to be the case (and does not occur for aluminium or Plexiglas plates).

Finally, for Plexiglas plates we have

$$k_0 \approx (fh)^{1/2} \times \begin{cases} 0.198\,37, & \text{in air,} \\ 0.045\,49, & \text{in water.} \end{cases} \tag{5.18}$$

As found before, the plate of Plexiglas construction in air has subsonic unattenuated edge waves for a wide range of values of $f \times h$ (bounded above by $f \times h < 25.5$ m s^{-1}). For example, a plate of thickness $h = 2$ cm has a non-dimensionalized edge-wave wavenumber of $k \approx 1.003\,796$ at frequency 1 KHz. As found before, in water the unattenuated edge waves on Plexiglas are found to be cut off for all values of $f \times h$.

It is apparent from the numerical results that the edge wave exists only for configurations with very small non-dimensional fluid loading ϵ. It is natural to enquire whether there is an upper bound on ϵ above which the edge wave cannot exist at any frequency. A search was made by varying k_0 and finding the value of ϵ at which $k = k_f$, that is, for example, for $k_0 = 0.8$ and $\nu = 0.334$ the point of intersection of the curves in figure 4. The graph of ϵ versus k_0 in figure 7 for $\nu = 0.33$ indicates that the upper bound for this value of Poisson's ratio is $\epsilon \approx 0.0462$ and it occurs at $k_0 \approx 0.59$, or $f = 0.35 f_c$. The three plate materials considered all have approximately the same Poisson's ratio, close to $\nu \approx 0.33$. Hence, referring to the values of ϵ in table 2, they should all exhibit edge waves in air because $\epsilon < 0.046$ for each plate material, but none permit edge waves in water because $\epsilon > 0.046$ in each case. This agrees with the specific numerical findings for the three materials above.

The upper bound on ϵ of course depends upon the value of ν. It tends to zero as $\nu \to 0$, and increases for values of ν greater than the value 0.33 considered in figure 7. However, it does not increase much beyond the small value 0.0462. We

suggest that the order of magnitude of this limiting fluid-loading value probably scales as ν^4 for the following reason. Referring to (3.23) for the fluid-loaded plate wavenumber k_{f}, it follows that k_{f} achieves a minimum value of $k_{\mathrm{f,min}}$ as a function of k_0 at $k_0 = k_{\mathrm{f,min}}/\sqrt{2}$, where $k_{\mathrm{f,min}}$ satisfies

$$k_{\mathrm{f,min}}^4 - 1 - \frac{4\epsilon}{k_{\mathrm{f,min}}^2} = 0. \tag{5.19}$$

Now, for light fluid loading it can be expected that the fluid-coupled plate wavenumber, k_{f}, is not too far in value from the *in vacuo* edge-wave wavenumber k_{v} of (5.6). Hence,

$$\epsilon = (k_{\mathrm{v}}^4 - 1)k_{\mathrm{v}}^2/4 \approx (k_{\mathrm{f,min}}^4 - 1)k_{\mathrm{f,min}}^2/4. \tag{5.20}$$

The *in vacuo* wavenumber depends only upon ν, and so expanding the right member in (5.20) gives a rough idea that edge waves exist as long as ϵ is less than about

$$\epsilon = \tfrac{1}{16}\nu^4 + \mathcal{O}(\nu^6). \tag{5.21}$$

Hence, for small ϵ the minimum fluid-loaded wavenumber, of (5.19), becomes

$$k_{\mathrm{f,min}} = 1 + \epsilon + \mathcal{O}(\epsilon^2), \tag{5.22}$$

and it occurs at $k_0 = 1/\sqrt{2}+\mathcal{O}(\epsilon)$, or $f = 0.5f_{\mathrm{c}}+\mathcal{O}(\epsilon)$. So, to summarize, the *in vacuo* edge-wave wavenumber k_{v} and the fluid-loaded plate wavenumber are comparable if $\epsilon = \mathcal{O}(\nu^4)$, and the wavenumbers are closest at $k_0 \approx 0.7$. This scaling suggests that, as $\nu \to 0$, the range of possible ϵ under which edge waves exist will shrink rapidly.

   Finally, it is interesting to find that the range of permissible fluid loading is determined by the Poisson's ratio of the plate material alone, and not by any other material parameter. This is, in a sense, a consequence of the fact that the edge wave *in vacuo* is really a Poisson effect (Thurston & McKenna 1974). Thus, the flexural wave in materials with zero Poisson's ratio automatically satisfies the free edge conditions, and is then not strictly an edge wave because it does not decay with distance from the edge. Conversely, the edge wave exists because of the Poisson effect when ν is non-zero.

6. Conclusions

This project was originally started in order to answer the question 'do edge waves propagate without attenuation along the edge of a thin elastic plate under fluid loading?'. It was certainly not clear to the authors at the outset what the answer was going to be. On the one hand, straight-crested (i.e. two-dimensional) flexural waves are unattenuated by the presence of an embedding fluid, but, on the other, edges are known to be efficient scatterers of acoustical/vibrational energy. For the edge wave to persist, it is necessary for the acoustic field in the fluid to decay to zero as one moves radially outwards in any direction perpendicular to the plate edge. From expression (4.10), this occurs as long as the wavenumber k is real and greater than k_0, and θ_4, θ_3^*, θ_3^{**} are real. Further, the plate deflection must also decay to zero at large distances from the plate edge, i.e. the energy from the edge wave must not be transferred into the creation of flexural waves propagating in the

direction orthogonal to the edge. The above question can now be answered definitively: this article has shown, by analytical means, that flexural edge waves can exist under limited but practical combinations of plate material and exterior fluid. These conditions are restricted to very light fluid loading: air on metal for instance. In none of the examples considered is it possible for the edge wave to exist in water. Nevertheless, the existence of the edge wave in air could have interesting ramifications. It means that edge waves can propagate on thin plates without radiating any of their energy into the surrounding fluid, and, consequently, the structural vibrational energy can persist for relatively long periods (attenuated only by mechanical damping). This phenomenon could very well play a role in the acoustical properties of many common structures in air, e.g. percussion instruments such as cymbals. Structures composed of thin plates or shells that, *in vacuo*, resonate at certain frequencies, may, when immersed in a fluid, demonstrate zero radiation damping at these frequencies. One example is the musical saw (Scott & Woodhouse 1992), which has a standing wave, or trapped mode, along the saw's length due to imposed curvature (in fact around a point of inflection). It is interesting to speculate on the possibility of zero radiation damping for this structure for sufficiently light fluid loading!

As a final point to note, although the existence of the edge wave on submerged thin plates has been established herein by theoretical means, it remains to be demonstrated in practice. Perhaps somewhat surprisingly, this is in direct contrast to results in the literature for wedge acoustic waves, that is, waves propagating along the tip of a wedge-shaped elastic body submerged in a fluid. This model problem has been investigated by experimentalists (see, for example, Chamuel 1996), but is only amenable to theoretical study via asymptotic or numerical, rather than exact, approaches. Thus, the work of Krylov (1998), Hladky-Hennion *et al.* (1997) and others on travelling edge waves on wedges in water presume, *but do not prove*, their existence in such circumstances. Indeed, the present study would suggest that for wedges of shallow angle it is most unlikely to find edge waves propagating without attenuation. Krylov's (1998) approach, which employs an approximation based on ray theory for slender wedges, does not take into account the diffraction effects (in a direction perpendicular to the edge) of the semi-infinite body on the edge-wave energy, and so is unlikely to be able to predict cut-off of real propagating wavenumbers as fluid loading increases. The authors believe that the observations made in this paper add to existing theoretical studies in this regard, and would welcome further experimental investigations both to compare with the predictions of the present theory and to determine cut-off values for unattenuated fluid-loaded wedge waves.

References

Abrahams, I. D. 1981 Scattering of sound by a heavily loaded finite elastic plate. *Proc. R. Soc. Lond.* A **378**, 89–117.

Cannell, P. A. 1976 Acoustic edge scattering by a heavily loaded elastic half-plane. *Proc. R. Soc. Lond.* A **350**, 71–89.

Chamuel, J. R. 1996 Flexural edge waves along free and immersed elastic waveguides. In *Review of Progress in Quantitative Nondestructive Evaluation, Proc. 16th Symp. Quantitative Nondestructive Evaluation, Brunswick, Maine, 28 July 1996* (ed. D. O. Thompson & D. E. Chimenti), vol. 16, pp. 129–136. New York: Plenum.

Graff, K. F. 1975 *Wave motion in elastic solids*. New York: Dover.

Hladky-Hennion, A.-C., Langlet, P. & de Billy, M. 1997 Finite element analysis of the propagation of acoustic waves along waveguides immersed in water. *J. Sound Vib.* **200**, 519–530.

Junger, M. C. & Feit, D. 1986 *Sound, structures and their interaction*. Cambridge, MA: MIT Press.

Konenkov, Yu. K. 1960 A Rayleigh-type flexural wave. *Sov. Phys. Acoust.* **6**, 122–123.

Krylov, V. V. 1998 On the velocities of localized vibration modes in immersed solid wedges. *J. Acoust. Soc. Am.* **103**, 767–770.

Lagasse, P. E. & Oliner, A. A. 1976 Acoustic flexural mode on a ridge of semi-infinite height. *Electron. Lett.* **12**, 11–13.

Noble, B. 1988 *The Wiener–Hopf technique*, 2nd edn. New York: Chelsea.

Norris, A. N. 1994 Flexural edge waves. *J. Sound Vib.* **171**, 571–573.

Norris, A. N., Krylov, V. V. & Abrahams, I. D. 2000 Flexural edge waves and comments on 'A new bending wave solution for the classical plate equation' (*J. Acoust. Soc. Am.* **104**, 2220–2222). *J. Acoust. Soc. Am.* **107**, 1781–1784.

Scott, J. F. M. & Woodhouse, J. 1992 Vibration of an elastic strip with varying curvature. *Phil. Trans. R. Soc. Lond.* A **339**, 587–625.

Sinha, B. K. 1974 Some remarks on propagation characteristics of ridge guides for acoustic waves at low frequencies. *J. Acoust. Soc. Am.* **56**, 16–18.

Thurston, R. N. & McKenna, J. 1974 Flexural acoustic waves along the edge of a plate. *IEEE Trans. Sonics Ultrason.* **21**, 296–297.